

# Quantum chaos in multicharged ions and statistical approach to the calculation of electron-ion resonant radiative recombination

G. F. Gribakin, A. A. Gribakina, and V. V. Flambaum

*School of Physics, The University of New South Wales, Sydney 2052, Australia*

(July 8, 2021)

## Abstract

We show that the spectrum and eigenstates of open-shell multicharged atomic ions near the ionization threshold are chaotic, as a result of extremely high level densities of multiply excited electron states ( $10^3 \text{ eV}^{-1}$  in  $\text{Au}^{24+}$ ) and strong configuration mixing. This complexity enables one to use statistical methods to analyse the system. We examine the dependence of the orbital occupation numbers and single-particle energies on the excitation energy of the system, and show that the occupation numbers are described by the Fermi-Dirac distribution, and temperature and chemical potential can be introduced. The Fermi-Dirac temperature is close to the temperature defined through the canonical distribution. Using a statistical approach we estimate the contribution of multielectron resonant states to the radiative capture of low-energy electrons by  $\text{Au}^{25+}$  and demonstrate that this mechanism fully accounts for the  $10^2$  times enhancement of the recombination over the direct radiative recombination, in agreement with recent experimental observations.

PACS numbers: 31.50.+w, 34.80.Lx, 32.70.Cs, 05.30.Fk

## I. INTRODUCTION

In this paper we investigate the spectrum and eigenstates of a multicharged positive ion at energies close to its ionization threshold  $I$ . Using  $\text{Au}^{24+}$  ( $I = 750$  eV) as an example, we show that this spectrum is dominated by multiple electron excitations into a few low-lying unoccupied orbitals. As a result, it is extremely dense, with level spacings  $\sim 1$  meV between the states of a given total angular momentum and parity  $J^\pi$ . The electron Coulomb interaction induces strong mixing of the multiply-excited configurations, which leads to a statistical equilibrium in the system. The latter is similar to a thermal equilibrium, and variables such as temperature can be introduced to describe it. This enables one to use a statistical approach in the situation where a full dynamical quantum calculation is simply impossible because of the enormous size of the Hilbert space ( $\gtrsim 10^5$  for  $\text{Au}^{24+}$ ).

We apply this approach to the problem of radiative capture of low-energy electrons by multicharged positive ions, and show that in these systems the contribution of resonant *multielectronic* recombination that proceeds via electron capture into the *multiply-excited* compound states, is responsible for high recombination rates, much greater than those expected from the simple direct radiative recombination. Our calculation resolves quantitatively the long-standing puzzle of huge enhancements of the electron-ion recombination rates, and essentially removes the “enormous discrepancies between theoretical and experimental rate coefficients” (Hoffknecht *et al.* 1998). The situation here turns out to be similar to the radiative neutron capture by complex nuclei [ $(n, \gamma)$  reaction] where the resonance mechanism involving the compound nucleus states is also much stronger than the direct capture (Flambaum and Sushkov 1984, 1985).

So far the enhancement of the recombination rates at low electron energies  $\lesssim 1$  eV has been observed for a number of ions<sup>1</sup>. Its magnitude ranges from a factor of about ten for  $\text{Ar}^{13+}$  (Gao *et al.* 1995),  $\text{Au}^{50+}$  and  $\text{Pb}^{53+}$  (Uwira *et al.* 1997a), and  $\text{U}^{28+}$  (Müller and Wolf 1997), to over a hundred for  $\text{Au}^{25+}$  (Hoffknecht *et al.* 1998). This enhancement is sensitive to the electronic structure of the target, e.g., the recombination rates of  $\text{Au}^{49+}$  and  $\text{Au}^{51+}$  are much smaller than that of  $\text{Au}^{50+}$  (Uwira *et al.* 1997a). For few-electron ions, e.g.,  $\text{C}^{4+}$ ,  $\text{Ne}^{7+}$  and  $\text{Ar}^{15+}$  the observed rates are described well by the sum of the direct and dielectronic recombination rates (Schennach *et al.* 1994, Zong *et al.* 1997, Schuch *et al.* 1997). In more complicated cases, like  $\text{U}^{28+}$  or  $\text{Au}^{25+}$ , the questions of what are the particular resonances just above the threshold and how they contribute to the recombination “remain a mystery” (Mitnik *et al.* 1998).

---

<sup>1</sup>Apart from the enhancement at eV energies due to many-electron processes, which is the subject of our work, there is another specific enhancement at electron energies below 1 meV. This enhancement increases with the charge of the ion, and is observed for all ions including fully stripped ones, see Gao *et al.* 1997 and Uwira *et al.* 1997b, and we do not consider it here.

## II. SPECTRUM AND EIGENSTATES OF AU<sup>24+</sup>

Let us consider the problem of electron recombination on Au<sup>25+</sup>. Due to electron correlations the low-energy electron can be captured into an excited state of the compound Au<sup>24+</sup> ion. This system is the main object of our analysis. Au<sup>24+</sup> has 55 electrons. Its ground state belongs to the  $1s^2 \dots 4f^9$  configuration. Figure 1 shows the energies of its relativistic orbitals  $nlj$  obtained in the relativistic Hartree-Fock calculation. All orbitals below the Fermi level,  $1s$  to  $4f$ , were obtained in the self-consistent calculation of the Au<sup>24+</sup> ground state. Each of the excited orbitals above the Fermi level –  $5s$ ,  $5p$ , etc., was calculated by placing one electron into it, in the field of the frozen  $1s^2 \dots 4f^8$  core. The energy of the highest orbital occupied in the ground state is  $\varepsilon_{4f_{7/2}} = -27.9$  a.u. This value gives an estimate of the ionization potential of Au<sup>24+</sup>:  $I \approx |\varepsilon_{4f_{7/2}}|$ . Our relativistic configuration-interaction (CI) calculation of the ground states of Au<sup>24+</sup> $4f^9$  and Au<sup>24+</sup> $4f^8$  shows that they are characterized by  $J = \frac{15}{2}$  and 6, and their total energies are  $-18792.36$  and  $-18764.80$  a.u., respectively. Thus, the ionization threshold of Au<sup>24+</sup> is  $I = 27.56$  a.u. = 750 eV, in agreement with Hoffknecht *et al.* 1998.

The excited states of the ion are generated by transferring one, two, three, etc. electrons from the ground state into empty orbitals above the Fermi level (Fig. 1), or into the partially occupied  $4f$  orbitals. We are interested in the excitation spectrum of Au<sup>24+</sup> near its ionization threshold. This energy (27.5 a.u.) is sufficient to push up a few of the nine  $4f$  electrons, and even excite one or two electrons from the  $4d$  orbital. However, the preceding  $4p$  orbital is already deep enough to be considered inactive. Thus, we treat Au<sup>24+</sup> as a system of  $n = 19$  electrons above the frozen Kr-like  $1s^2 \dots 4p^6$  core. Note also that infinite Rydberg series corresponding to the excitations of one electron in the field of Au<sup>25+</sup> belong to the single-particle aspect of the Au<sup>25+</sup> +  $e^-$  problem, and we do not consider them here.

The number of multielectron states obtained by distributing 19 electrons over 31 relativistic orbitals,  $4d_{3/2}$  through to  $7g_{9/2}$ , is enormous, even if we are only interested in the excitation energies below 27.5 a.u. It is impossible to perform any CI calculation for them. However, there is another simpler way to analyse the spectrum. The scale of the configuration interaction strength is determined by the two-body Coulomb matrix elements which transfer electrons between different configurations. Their typical size in neutral atoms is  $\sim 1$  eV, and in Au<sup>24+</sup> it is about 1 a.u., which is roughly 25 times greater, due to the smaller radius of the ion. This scale is much smaller than  $I$ . Configuration mixing aside, the CI does not shift the mean energies of the configurations. Therefore, we can construct the excitation spectrum of Au<sup>24+</sup> by calculating the mean energies  $E_i$  of the configurations, and the numbers of many-electron states  $N_k$  within each of them:

$$E_i = E_{\text{core}} + \sum_a \epsilon_a n_a + \sum_{a \leq b} \frac{n_a(n_b - \delta_{ab})}{1 + \delta_{ab}} U_{ab} , \quad (1)$$

$$N_i = \prod_a \frac{g_a!}{n_a!(g_a - n_a)!} , \quad (2)$$

where  $n_a$  are the integer orbital occupation numbers of the relativistic orbitals in a given configuration ( $\sum_a n_a = n$ ),  $\epsilon_a = \langle a | H_{\text{core}} | a \rangle$  is the single-particle energy of the orbital  $a$  in the field of the core,  $g_a = 2j_a + 1$ , and  $U_{ab}$  are the average Coulomb matrix elements for the electrons in orbitals  $a$  and  $b$  (direct minus exchange):

$$U_{ab} = \frac{g_a}{g_a - \delta_{ab}} \left[ R_{abab}^{(0)} - \sum_{\lambda} \delta_p R_{abba}^{(\lambda)} \begin{pmatrix} j_a & j_b & \lambda \\ \frac{1}{2} & -\frac{1}{2} & 0 \end{pmatrix}^2 \right]. \quad (3)$$

Here  $R_{abba}^{(\lambda)}$  is the two-body radial Coulomb integral of  $\lambda$  multipole, and  $\delta_p = 1$  when  $l_a + l_b + \lambda$  is even, and 0 otherwise. The mean energy of the lowest configuration  $4d^{10}4f_{5/2}^6 4f_{7/2}^3$  obtained from Eq. (1) is just 0.28 a.u. above the CI ground state.

Using Eqs. (1)–(3) we find that there are 9000 configurations within 35 a.u. of the  $\text{Au}^{24+}$  ground state. They comprise a total of  $2.1 \times 10^8$  many-electron states. If we allow for about 10 different values of  $J$ ,  $2J + 1$  values of  $J_z$  and the two parities, there would still be about  $5 \times 10^5$  states in each  $J^\pi$  manifold. In Fig. 2 we show the total density of states for  $\text{Au}^{24+}$  as a function of  $\sqrt{E}$ , where  $E$  is the excitation energy of the system above the ground state. It is obtained by smoothing out the small-scale fluctuations of the level density

$$\rho(E) = \sum_i N_i \delta(E - E_i) \quad (4)$$

by folding it with a Gaussian with 1 a.u. variance. In reality this averaging is done by the interaction and mixing of the configurations (Flambaum *et al.* 1994), but the result is expected to be the same. The inset on Fig. 2 presents a break-up of the total density near the ionization threshold into the densities of states with given  $J$ :  $\rho(E) = \sum_J (2J + 1) \rho_J(E)$ . The most abundant values are  $J = \frac{5}{2}$  to  $\frac{15}{2}$ . For a given parity the density of such states at  $E \approx I$  is  $\rho_{J^\pi} \approx 3.5 \times 10^4$  a.u., which corresponds to the mean level spacing  $D = 1/\rho_{J^\pi} \sim 1$  meV. Figure 2 demonstrates the characteristic  $\rho \propto \exp(a\sqrt{E})$  behaviour of the level density predicted by the Fermi-gas model (Bohr and Mottelson 1969), where  $a$  is related to the single-particle level density at the Fermi level  $g(\varepsilon_F)$  as  $a = [2\pi^2 g(\varepsilon_F)/3]^{1/2}$ .  $g(\varepsilon_F) = 3a^2/2\pi^2$ . We obtain an accurate fit of the level density at  $E > 1$  a.u. by using a Fermi-gas model ansatz

$$\rho(E) = AE^{-\nu} \exp(a\sqrt{E}), \quad (5)$$

with  $A = 31.6$ ,  $\nu = 1.56$ , and  $a = 3.35$ . The corresponding value of  $g(\varepsilon_F) = 3a^2/2\pi^2 = 1.7$  a.u. is close to what one obtains from the Hartree-Fock orbital spectrum in Fig. 1. The other two parameters are different from the non-interacting Fermi-gas model values  $A = 1/\sqrt{48}$  and  $\nu = 1$ . The latter values in fact lead to strong underestimation of the level density. For most abundant  $J^\pi$  states the density  $\rho_{J^\pi}(E)$  is given by Eq. (5) with  $A_{J^\pi} \approx 0.15$ .

At first sight the huge level density makes the spectrum of  $\text{Au}^{24+}$  enormously complicated. On the other hand, this complexity enables one to analyse the system using statistical methods. The interaction between multiply-excited configuration states mixes them completely, and they lose their individual features. In this regime the spectral statistics become close to those of a random matrix ensemble, the eigenstates cannot be characterized by any quantum numbers except the exact ones (energy and  $J^\pi$ ), and the orbital occupation numbers deviate prominently from integers. This regime can be described as *many-body quantum chaos*. We have extensively studied it in direct numerical calculations for the rare-earth atom of Ce – a system with four valence electrons (Flambaum *et al.* 1994, 1996, 1998a, 1998b, Gribakina *et al.* 1995).

The strength of the configuration mixing is characterized by the spreading width  $\Gamma_{\text{spr}}$ . For a configuration basis state  $\Phi_k$  with energy  $E_k$  it defines the energy range  $|E - E_k| \lesssim \Gamma_{\text{spr}}$

of eigenstates in which this basis state noticeably participates. By the same token it shows that a particular eigenstate  $\Psi = \sum_k C_k \Phi_k$  contains a large number  $N \sim \Gamma_{\text{spr}}/D$  of *principal components* – basis states characterized by  $C_k \sim 1/\sqrt{N}$ . Outside the spreading width  $C_k$  decrease. This effect is usually referred to as *localization*. Apart from this,  $C_k$  behave closely to Gaussian random variables (Flambaum *et al.* 1994). The effect of spreading is approximated well by the Breit-Wigner shape of the mean-squared components (Bohr and Mottelson 1969)

$$\overline{C_k^2}(E) = \frac{1}{N} \frac{\Gamma_{\text{spr}}^2/4}{(E_k - E)^2 + \Gamma_{\text{spr}}^2/4}. \quad (6)$$

The normalization  $\sum_k \overline{C_k^2} = 1$  yields  $N = \pi\Gamma/2D$ . In systems with small level spacings  $D$  the number of principal components  $N$  can be very large. It reaches several hundreds in Ce, and can be as large as  $10^6$  in complex nuclei. At  $|E_k - E| > \Gamma$  Eq. (6) gives  $\overline{C_k^2}(E) \propto 1/(E_k - E)^2$ , which corresponds to the simple first-order perturbation theory dependence with constant mean-squared mixing matrix elements. In real systems the mixing between distant (in the sense of their unperturbed energies) basis states is usually suppressed. Accordingly, the Hamiltonian matrix is characterized by certain bandedness, i.e., the off-diagonal matrix elements  $H_{ij}$  decrease as one moves away from the main diagonal  $i = j$  (Gribakina *et al.* 1995). This causes a faster, close to exponential, decrease of the mean-squared components at large  $|E_k - E|$  (Flambaum *et al.* 1994).

In Fig. 3 we illustrate the behaviour of the eigenstate components by the results of a CI calculation which includes just two odd configurations of  $\text{Au}^{24+}$  with energies close to the ionization threshold:  $4f_{5/2}^3 4f_{7/2}^3 5p_{1/2} 5p_{3/2} 5f_{7/2}$  and  $4f_{5/2}^3 4f_{7/2}^3 5p_{1/2} 5d_{3/2} 5g_{7/2}$ . These two configurations produce a total of 143360 many-electron states with  $J$  ranging from  $\frac{1}{2}$  to 17.5. As an example we present the results obtained by diagonalization of the Hamiltonian matrix for  $J^\pi = \frac{13}{2}^-$ . This total angular momentum value is among the most abundant in the spectrum, as there are 1254  $J^\pi = \frac{13}{2}^-$  states. The mixing of the two configurations included is practically complete, since the weight of each configuration in every eigenstate is close to 50%, Fig. 4. Shown in the upper part of Fig. 3 are the components of the 590th eigenstate from the middle of the two-configuration spectrum. Both the fluctuations of  $C_k$  as function of basis state  $k$ , and the localization of the eigenstate components in the vicinity of the corresponding eigenvalue ( $E = 27.51$  a.u. above the  $\text{Au}^{24+}$  ground state) are evident.

A Breit-Wigner fit of the mean-squared components yields  $N = 975$  and  $\Gamma_{\text{spr}} = 0.50$  a.u., see lower part of Fig. 3. When the calculations are performed for one of the above configurations,  $N$  is about two times smaller, but  $\Gamma_{\text{spr}}$  is practically the same. The spreading width is related to the mean-squared off-diagonal Hamiltonian matrix element and the mean level spacing as  $\Gamma_{\text{spr}} \simeq 2\pi \overline{H_{ij}^2}/D$  (Bohr and Mottelson 1969). It is known to be a robust characteristic of the system. When more configurations are included, both  $D$  and  $\overline{H_{ij}^2}$  decrease, whereas  $\Gamma_{\text{spr}}$  does not change much. If one could do a full-scale CI calculation near the ionization threshold of  $\text{Au}^{24+}$  one would obtain eigenstates with  $N = (\pi/2)\Gamma_{\text{spr}}\rho_{J^\pi} \sim 3 \times 10^4$  principal components.

### III. STATISTICAL APPROACH

The spreading of the basis states due to configuration interaction introduces natural statistical averaging in the system. Based on this averaging, a statistical theory of finite Fermi systems of interacting particles can be developed (Flambaum and Izrailev 1997a, 1997b). It enables one to calculate various properties of the system as sums over the basis states, without actually diagonalizing the Hamiltonian matrix. For example, the mean orbital occupations numbers can be obtained as

$$n_a(E) = \sum_k \overline{C_k^2}(E) n_a^{(k)} \quad (7)$$

where  $n_a^{(k)}$  is the occupation number of the orbital  $a$  in the basis state  $k$ . To demonstrate how it works we have used a simple Gaussian model spreading

$$\overline{C_k^2}(E) \propto \exp \left[ -\frac{(E_k - E)^2}{2\Delta_E^2} \right] \quad (8)$$

and calculated the mean orbital occupation numbers as functions of the excitation energy  $E$  using  $\Delta_E = 1$  a.u., Fig. 5. Of course, in our calculation we sum over the configurations, rather than the actual many-electron basis states, and use their mean energies and weights given by Eqs. (1) and (2), cf. Eq. (4).

The oscillatory dependence with the period of about 3–4 a.u. is due to the shell structure of the  $\text{Au}^{24+}$  ion, Fig. 1. As the excitation energy increases the oscillations die out. Apart from this the occupation numbers of the orbitals below the Fermi level ( $4d$  and  $4f$ ) decrease, and those above it ( $5s$ ,  $5p$ , etc.) increase, as one would expect in a Fermi system. It seems very natural to try to describe this behaviour in the spirit of statistical mechanics, by introducing temperature and applying the standard Fermi-Dirac (FD) distribution (Flambaum *et al.* 1998b). Temperature has long been used to describe highly excited nuclei, and the question of thermalization was investigated recently in numerical calculations for the  $s - d$  shell nuclear model (Horoi *et al.* 1995, Zelevinsky *et al.* 1996). Of course, temperature can always be used to describe the equilibrium of a macroscopic system that contains a large number of particles, or to describe a small system interacting with a heat bath. In what follows we are going to see if the notion of temperature can be applied to our isolated system with a small number of active particles. The total number of electrons in  $\text{Au}^{24+}$  is quite large, however most of them are *inactive* at the excitation energies at or below the ionization threshold.

The formula for the single-particle occupation numbers  $\nu_a = n_a/g_a$  ( $0 \leq \nu_a \leq 1$ )

$$\nu_a = \frac{1}{1 + \exp[(\varepsilon_a - \mu)/T]}, \quad (9)$$

at a given temperature  $T$  and chemical potential  $\mu$  depends on the single-particle orbital energies  $\varepsilon_a$ . These energies are well defined for non-interacting particles in a given potential. For interacting particles (electrons in an atom or ion) one can introduce single-particle orbitals and energies using a *mean field* approximation, e.g. the Hartree-Fock method. From this points of view we could use the orbital energies  $\varepsilon_a^{\text{HF}}$  found in the mean field of

the  $\text{Au}^{24+}$  ground state  $1s^2 \dots 4d^{10}4f^9$ , Fig. 1. However, they may only be suitable at low excitation energies, when the mean field is close to that of the ground-state  $\text{Au}^{24+}$ .

As the excitation energy increases the orbital occupation numbers change noticeably, as shown by Fig. 5. This gives rise to a change of the mean field, and as a result, the orbital energies are shifted by

$$\delta\varepsilon_a(E) = \sum_b U_{ab}\delta n_b(E) , \quad (10)$$

where  $\delta n_b = n_b(E) - n_b(0)$  is the difference between the occupation numbers at energy  $E$  and in the ground state at  $E = 0$ . Using our numerical energy-dependent occupation numbers we find the energy dependence of the orbital energies, shown for a few low-lying orbitals in Fig. 6. With the increase of the excitation energy the electrons are transferred into higher orbitals which have larger radii. Accordingly, the electron cloud becomes more diffuse, the screening of the nuclear potential is reduced, and the orbital energies go down. This effect is especially strong for the inner  $4d$  and  $4f$  orbitals. As we will see below the shift of the lower orbital energies is comparable with the temperature of the system, and it has to be taken into account when applying the FD formula.

In Fig. 7 we present the single-particle occupation numbers at five different excitation energies, as functions of the shifted orbital energies

$$\varepsilon_a(E) = \varepsilon_a(0) + \delta\varepsilon_a(E) , \quad (11)$$

where we take  $\varepsilon_a(0) = \varepsilon_a^{\text{HF}}$ . The numerical values agree well with the FD distribution Eq. (9), obtained by the least-square fits of the temperature  $T$  and chemical potential  $\mu$  (solid lines). Figures 8 and 9 present the dependence of  $\mu$  and the ‘‘Fermi-Dirac temperature’’  $T$  on the energy of the system (solid circles).

Occupation numbers aside, the relation between the temperature and energy can be defined by the level density  $\rho(E)$ , Eq. (4), through the canonical average

$$E(T) = \frac{\int e^{-E/T} E \rho(E) dE}{\int e^{-E/T} \rho(E) dE} = \frac{\sum_i E_i N_i e^{-E_i/T}}{\sum_i N_i e^{-E_i/T}} , \quad (12)$$

or from the statistical physics formula

$$T^{-1} = \frac{d \ln[\rho(E)]}{dE} , \quad (13)$$

using the smooth fit (5). The latter yields  $T \simeq 2\sqrt{E}/a$ , or  $E \propto T^2$ , characteristic of the Fermi systems. Figure 9 shows that for the energies above 3 a.u. all three definitions of temperature give close values. As is known, the expansion of the chemical potential in a Fermi system at small temperatures starts with a  $T^2$  term (Landau and Lifshitz 1969). Accordingly, its shift from the ground-state value is proportional to the energy. Indeed, a simple linear fit  $\mu = -27.6 - 0.094E$  closely follows the numerical values in Fig. 8.

If we use  $T(E)$  given by the canonical definition and the linear fit of  $\mu$ , together with the orbital energies [Eq. (11)], the FD formula gives smooth energy dependencies of the occupation numbers, see Fig. 5. They reproduce the behaviour of the numerical occupation numbers averaged over the shell-structure fluctuations.

#### IV. DIRECT AND RESONANT RECOMBINATION

Let us now estimate the direct and resonant contributions to the recombination rate of  $\text{Au}^{25+}$ . The direct radiative recombination cross section is estimated by introducing an effective ionic charge  $Z_i$  into the Kramers formula, which describes radiative electron capture in the Coulomb potential, see e.g. Sobelman 1992,

$$\sigma_n^{(d)} = \frac{32\pi}{3\sqrt{3}c^3} \frac{(Z_i^2 \text{Ryd})^2}{n\varepsilon(Z_i^2 \text{Ryd} + n^2\varepsilon)}, \quad (14)$$

where  $\varepsilon$  is the initial electron energy,  $n$  is the principal quantum number of the final electron state, and atomic units are used ( $\text{Ryd} = \frac{1}{2}$  a.u.). If we are interested in the total recombination cross section the sum over  $n$  must be calculated,

$$\sigma^{(d)} = \sum_n \sigma_n^{(d)}. \quad (15)$$

Due to the  $n^{-1}$  factor in Eq. (14) this sum diverges logarithmically, until values of  $n \sim n_{\text{max}}$  are reached, where  $n_{\text{max}}^2 \varepsilon = Z_i^2 \text{Ryd}$ , after which it converges rapidly. With the logarithmic accuracy the result is given by

$$\sigma^{(d)} \simeq \frac{32\pi}{3\sqrt{3}c^3} \frac{\text{Ryd}}{\varepsilon} Z_i^2 \ln \left( \frac{Z_i}{n_0} \sqrt{\frac{\text{Ryd}}{\varepsilon}} \right), \quad (16)$$

where  $n_0$  is the principal quantum number of the lowest unoccupied ionic orbital, which determines the lower limit in the summation over  $n$ . Using  $Z_i = 25$ ,  $n_0 = 5$  for electron recombination with  $\text{Au}^{25+}$ , and choosing a small electron energy of  $\varepsilon = 0.1$  eV we obtain  $\sigma^{(d)} \approx 7 \times 10^{-17}$  cm<sup>2</sup>. This corresponds to the recombination rate of  $\lambda = \sigma v = 1.3 \times 10^{-9}$  cm<sup>3</sup>s<sup>-1</sup>, which is two orders of magnitude smaller than the experimental  $\lambda = 1.8 \times 10^{-7}$  cm<sup>3</sup>s<sup>-1</sup> at this energy (Hoffknecht *et al.* 1998).

The electron energy of 0.1 eV is equal to the transversal temperature of the electron beam in the experiment, whereas the longitudinal temperature is much smaller, 1 meV. Therefore, to make estimates of the recombination rates at this and higher energies one can use the the cross sections without averaging over the Maxwellian velocity distribution. It is also important that the energy dependence of the experimental recombination rate is in agreement with that of the direct radiative capture for electron energies  $1 \text{ meV} < \varepsilon \lesssim 1$  eV. The latter is basically given by the  $1/\varepsilon$  factor in Eq. (16). The experimental data of Hoffknecht *et al.* (1998) is reproduced well by the direct radiative rate multiplied by a factor of 150.

The cross section of resonant radiative capture averaged over the resonances is (Landau and Lifshitz 1977)

$$\sigma^{(r)} = \frac{\pi^2}{\varepsilon} \frac{\Gamma_\gamma \Gamma_e}{D(\Gamma_\gamma + \Gamma_e)} \approx \frac{\pi^2}{\varepsilon} \frac{\Gamma_\gamma}{D} \quad (\Gamma_e \gg \Gamma_\gamma), \quad (17)$$

where  $\Gamma_\gamma$  and  $\Gamma_e$  are the mean radiative and autoionization (or elastic) widths of the resonances,  $D$  is the mean resonance spacing, and we drop the statistical weights of the initial and intermediate ionic states. The relation  $\Gamma_e \gg \Gamma_\gamma$  is usually valid for a few lower partial



waves, where the electron interaction is stronger than the electromagnetic one. Equation (17) is written for the electron  $s$ -wave, and the contributions of higher electron partial wave contain an extra factor  $(2l + 1)$ .

The radiative width of the resonant state at energy  $E \approx I$  is found by summing the partial widths for all lower-lying states  $E' = E - \omega$ ,

$$\Gamma_\gamma \approx \frac{3}{2J + 1} \int_0^I \frac{4\omega^3 |d_\omega|^2}{3c^3} \rho_{J\pi}(I - \omega) d\omega, \quad (18)$$

where the factor 3 accounts for  $J' = J, J \pm 1$ , and  $d_\omega$  is the reduced dipole matrix element between the many-electron states. Because of the chaotic structure of these states  $d_\omega$  is suppressed compared to the typical single-particle matrix element  $d_0$ :  $d_\omega \sim d_0/\sqrt{N}$  (Flambaum and Sushkov 1984a, Flambaum *et al.* 1994, 1996). This estimate for systems with dense chaotic spectra in fact follows from the dipole sum rule: the number of lines in the spectrum is large,  $\propto D^{-1} \propto N$ , consequently, the line strengths are small,  $|d_\omega|^2 \sim |d_0|^2 N^{-1}$ .

The integrand in Eq. (18) peaks strongly because of the competition between the  $\omega^3$  factor, and the level density  $\rho_{J\pi}(I - \omega)$  that drops quickly as we go down from the threshold, see Eq. (5). As a result, the integral can be evaluated by the saddle-point method. Using the statistical estimate of  $d_\omega$  we obtain

$$\sigma^{(r)} = \frac{8\pi d_0^2}{(2J + 1)c^3 \varepsilon \Gamma_{\text{spr}}} \sqrt{\frac{2\pi}{3}} \rho_{J\pi}(I - \omega_0) \omega_0^4, \quad (19)$$

where  $\omega_0 = 6\sqrt{I}/a$  corresponds to the maximum of the decay photon spectrum in Eq. (18). This cross section has the same energy dependence as  $\sigma^{(d)}$ . Hence, it is also in agreement with the energy dependence observed in the experiment, and we can estimate its magnitude at one particular electron energy, e.g., 0.1 eV. To do this we use a simple estimate of the single-particle dipole matrix elements in the ion with charge  $Z_i$ :  $d_0 \sim Z_i^{-1}$ , together with  $2J + 1 \approx 10$ , and substitute  $\Gamma_{\text{spr}} = 0.5$ ,  $\omega_0 = 9.4$ , and  $\rho_{J\pi}(I - \omega_0) = 2.5 \times 10^3$  a.u. into Eq. (19). At  $\varepsilon = 0.1$  eV this gives  $\sigma^{(r)} = 7 \times 10^{-16}$  cm<sup>2</sup>, therefore,  $\sigma^{(r)}/\sigma^{(d)} = 10$ , and we obtain a factor of ten enhancement over the direct recombination due to radiative capture into multiply excited resonant states (the corresponding radiative width is  $\Gamma_\gamma = 2 \times 10^{-7}$  a.u.). It comes from the large effective number of final states in the radiative width in Eq. (18) (numerically  $\Gamma_\gamma \sim 2 \times 10^{-7}$  a.u.). This enhancement has been obtained for the electron  $s$ -wave. The contributions of higher electron partial waves are similar to Eq. (17) times  $(2l + 1)$ . Therefore, a few lower partial waves ( $s, p, d$ ) produce resonant cross section values  $10^2$  times greater than  $\sigma^{(d)}$ , which matches the experimentally observed values. With the increase of the orbital angular momentum  $l$  of the electron the capture width  $\Gamma_e$  becomes smaller than the radiative width, and the contribution of the higher partial waves to the resonant cross section is suppressed.

## V. CONCLUSIONS

In summary, the resonant radiative capture mechanism fully explains the strongly enhanced recombination rates observed for eV electrons on multicharged ions. Its origin is in the high level densities of chaotic multiply-excited electron states in multicharged ions. The

size of the enhancement is sensitive to the electron structure of the ion, which determines the level density. We have shown that a statistical approach can be applied to the analysis of this complex system. One can also use a statistical theory to calculate mean-squared matrix elements between multiply excited chaotic states in terms of single-particle amplitudes, occupation numbers,  $\Gamma_{\text{spr}}$  and  $D$  (Flambaum and Vorov 1993, Flambaum *et al.* 1994, 1996), and obtain accurate quantitative information about the processes involving chaotic states and resonances. At higher electron energies the resonant capture proceeds via so-called doorway states (Bohr and Mottelson 1969) – simple dielectronic autoionizing states, which are then “fragmented” into the dense spectrum of multiply-excited resonances (see Mitnik *et al.* 1998, Flambaum *et al.* 1996 and Refs. therein).

## REFERENCES

- Bohr, A., and B. Mottelson, B. (1969). ‘Nuclear structure’, Vol. 1 (Benjamin: New York).
- Flambaum, V. V., and Sushkov, O. P. (1984). *Nucl. Phys. A* **412**, 13.
- Flambaum, V. V., and Sushkov, O. P. (1985). *Nucl. Phys. A* **435**, 352.
- Flambaum, V. V., and Vorov, O. K. (1993). *Phys. Rev. Lett.* **70**, 4051.
- Flambaum, V. V., Gribakina, A. A., Gribakin, G. F., and Kozlov, M. G. (1994). *Phys. Rev. A* **50**, 267.
- Flambaum, V. V., Gribakina, A. A., and Gribakin, G. F. (1996). *Phys. Rev. A* **54**, 2066.
- Flambaum, V. V., and Izrailev, F. M. (1997a). *Phys. Rev. E* **55**, R13.
- Flambaum, V. V., and Izrailev, F. M. (1997b). *Phys. Rev. E* **56**, 5144.
- Flambaum, V. V., Gribakina, A. A., and Gribakin, G. F. (1998). *Phys. Rev. A* **58**, 230.
- Flambaum, V. V., Gribakina, A. A., Gribakin, G. F., and Ponomarev, I. V. (1998). *Phys. Rev. E* **57**, 4933.
- Gao, H., *et al.* (1995). *Phys. Rev. Lett.* **75**, 4381.
- Gao, H., *et al.* (1997). *J. Phys. B* **30**, L499 (1997).
- Gribakina, A. A., Flambaum, V. V., and Gribakin, G. F. (1995). *Phys. Rev. E* **52**, 5667.
- Hoffknecht A., *et al.* (1998). *J. Phys. B* **31**, 2415.
- Horoi, M., Zelevinsky, V., and Brown, B. A. (1995). *Phys. Rev. Lett.* **74**, 5194.
- Landau, L. D., and Lifshitz, E. M. (1969). ‘Statistical Physics’ (Pergamon Press: New York).
- Landau, L. D., and Lifshitz, E. M. (1977). ‘Quantum Mechanics’, Ch. 18 (Pergamon Press: Oxford).
- Mitnik, D. M., *et al.* (1998). *Phys. Rev. A* **57**, 4365.
- Müller, A., and Wolf, A. (1997). *Hyperfine Interact.* **109**, 233.
- Schennach, S., *et al.* (1994). *Z. Phys. D* **30**, 291.
- Schuch, R., *et al.* (1997). *Phys. Scripta* **T73**, 114.
- Sobelman, I. I. (1992). ‘Atomic Spectra and Radiative Transitions’ (Springer: Berlin).
- Uwira, O., *et al.* (1997a). *Hyperfine Interact.* **108**, 149.
- Uwira, O., *et al.* (1997b). *Hyperfine Interact.* **108**, 167.
- Zelevinsky, V., Brown, B. A., Frazier, N., and Horoi, M. (1996). *Phys. Rep.* **276**, 85.
- Zong, W., *et al.* (1997). *Phys. Rev. A* **56**, 386.

FIGURES

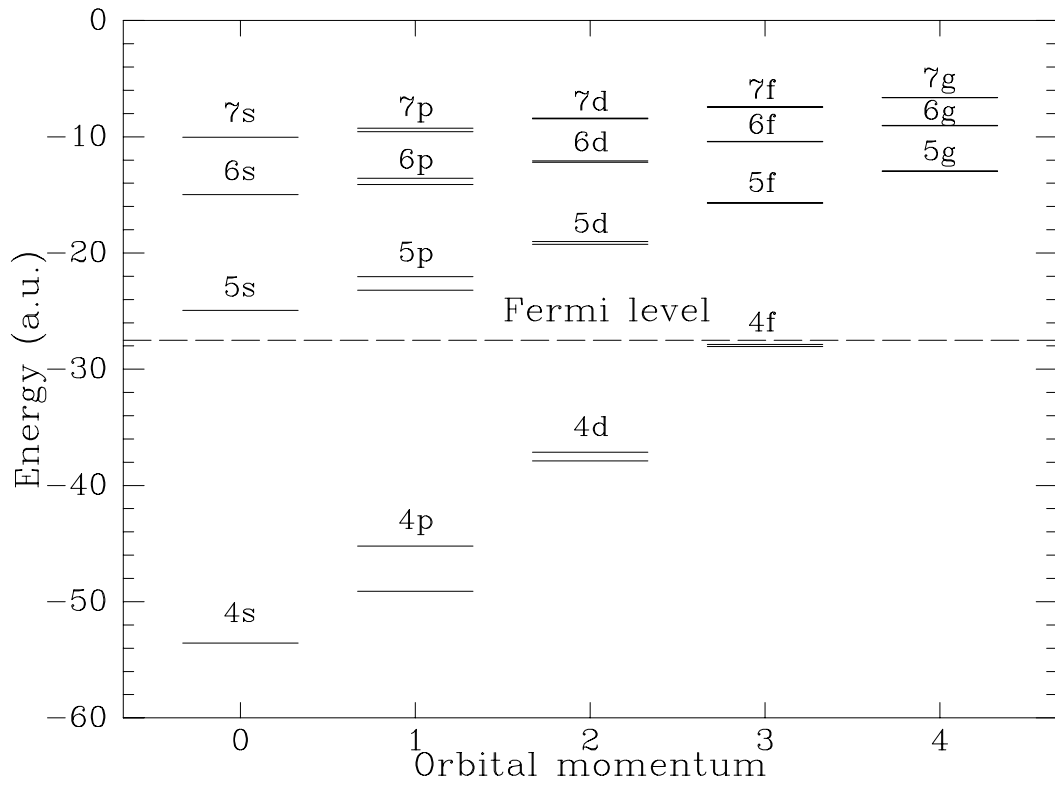


FIG. 1. Electron orbitals of  $\text{Au}^{24+}$  from the relativistic Hartree-Fock calculation.

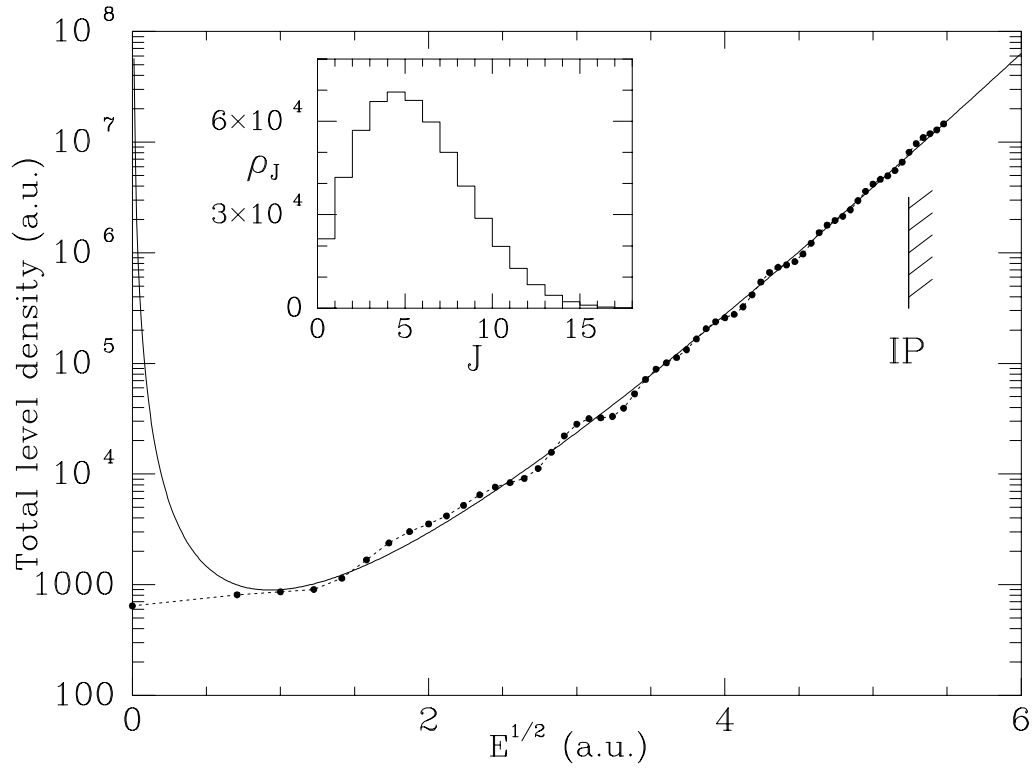


FIG. 2. Level density in  $\text{Au}^{24+}$ . Full circles connected by dotted line to guide the eye is the result of our numerical calculation. Solid line is the analytical fit, Eq. (5). The inset shows the densities of states with different  $J$  near the ionization threshold  $E = I$ .

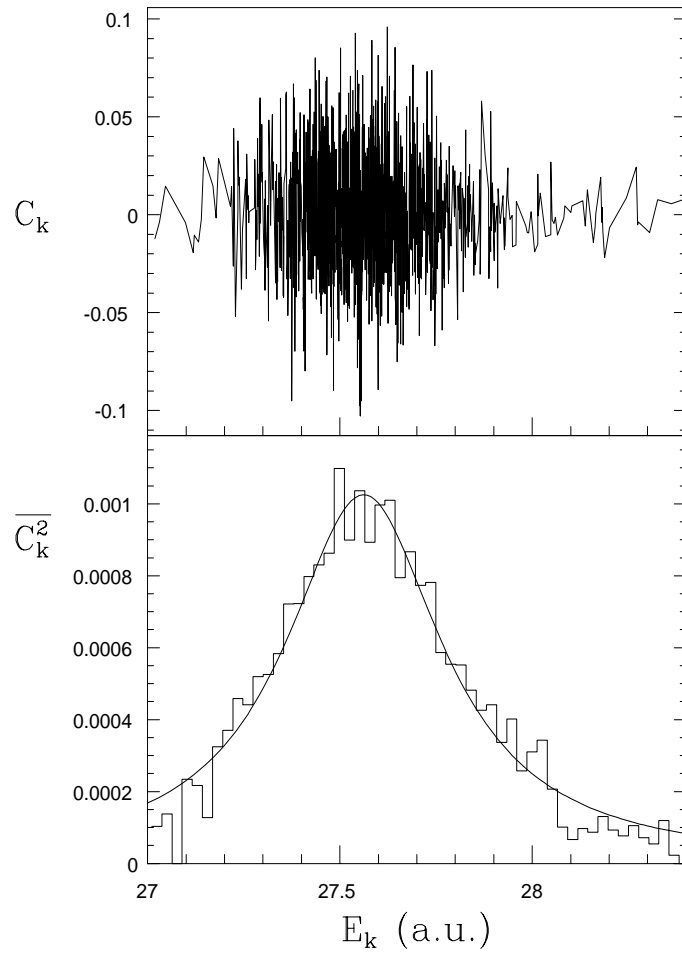


FIG. 3. Components of the 590th  $J^\pi = \frac{13}{2}^-$  eigenstate from a two-configuration calculation (top), and a fit of  $\overline{C_k^2}(E)$  by the Breit-Wigner formula (6) (bottom).

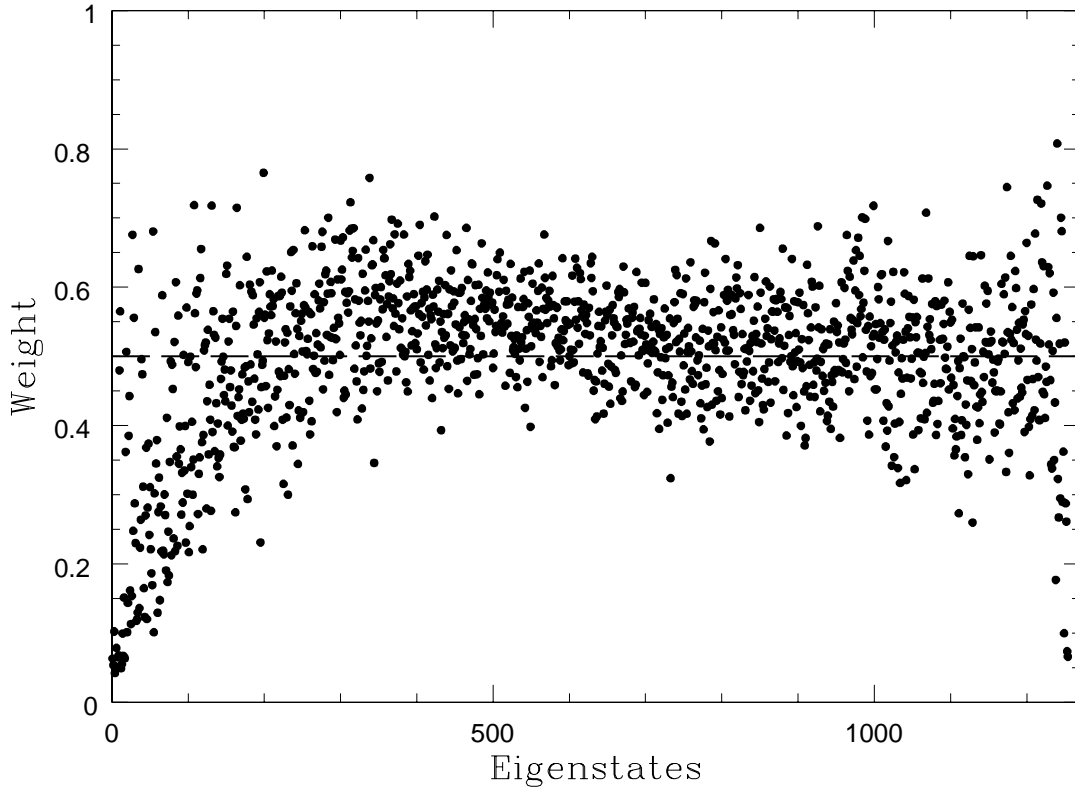


FIG. 4. Weights of the  $4f_{5/2}^3 4f_{7/2}^3 5p_{1/2} 5p_{3/2} 5f_{7/2}$  configuration in the  $J^\pi = \frac{13}{2}^-$  eigenstates obtained in the two-configuration calculation. Note that for a few lower eigenstates the weights of this configuration are small, because its mean energy is about 0.03 a.u. higher than that of the other configuration.

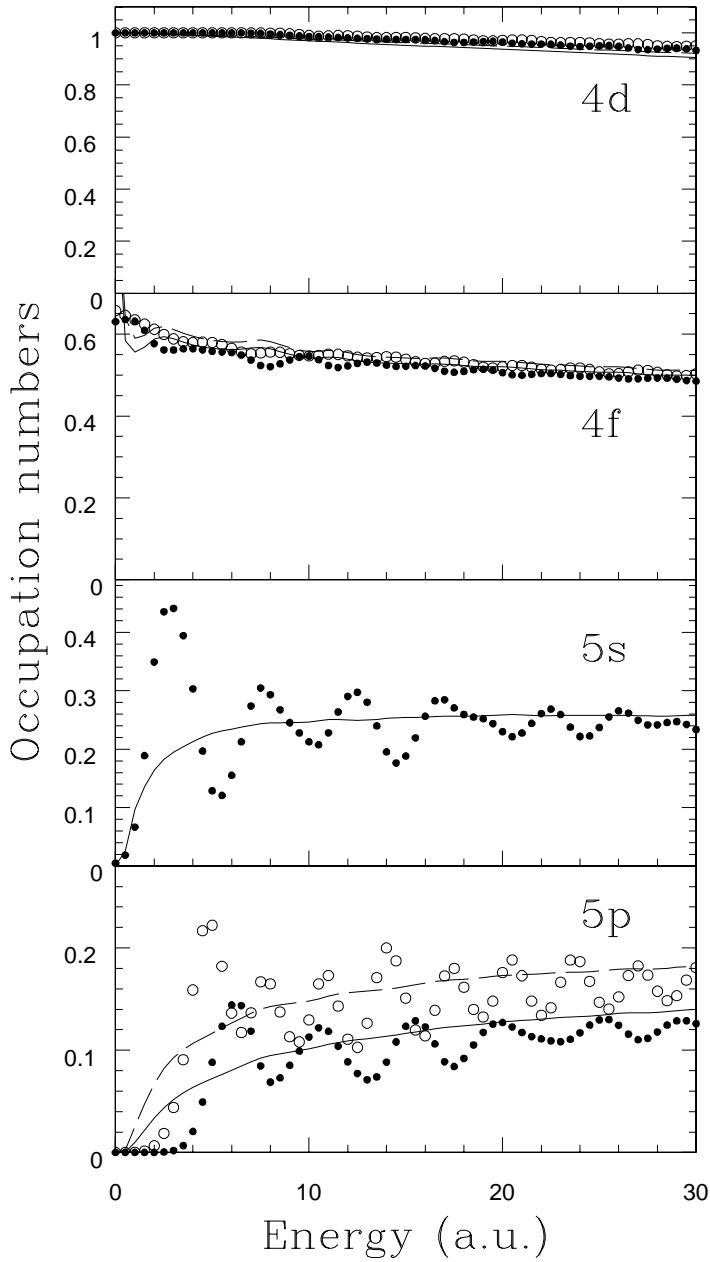


FIG. 5. Energy dependence of the single-particle occupation numbers  $n_a/g_a$  calculated numerically from Eq. (7) for  $4d$ ,  $4f$ ,  $5s$  and  $5p$  orbitals: solid and open circles correspond to  $j = l \pm \frac{1}{2}$  subshells, respectively. Solid and dashed lines ( $j = l \pm \frac{1}{2}$ , respectively) show the results obtained from the FD formula using the energy-dependent orbital energies and chemical potential, and the canonical relation between the temperature and the excitation energy (solid line in Fig. 9).



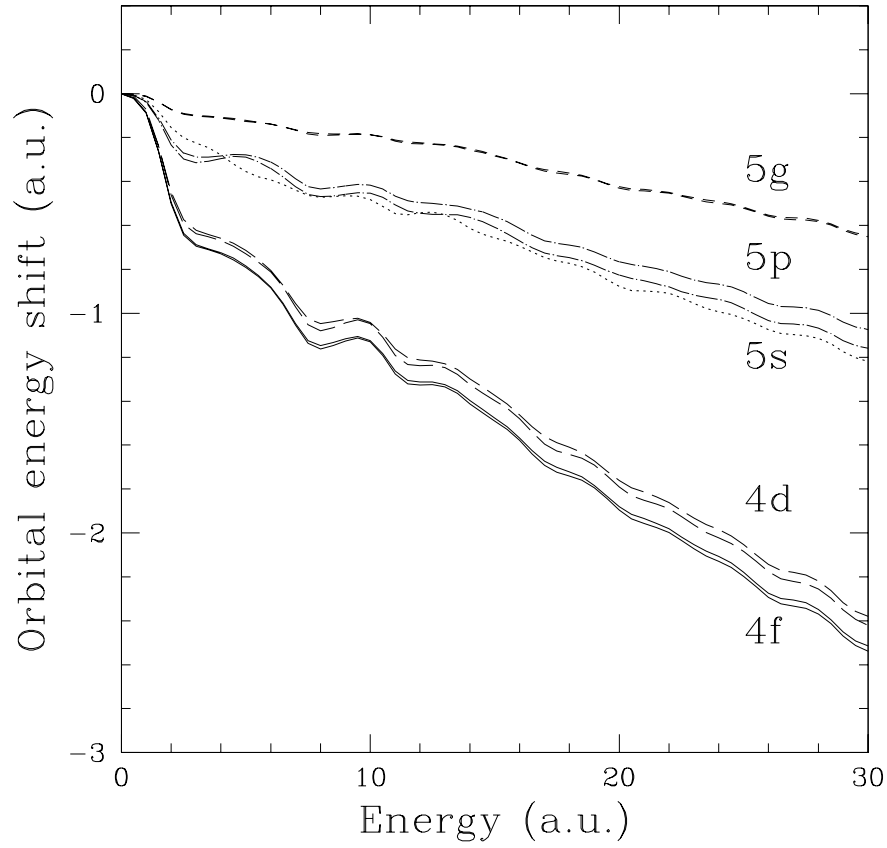


FIG. 6. Shifts of the single-particle orbital energies, Eq. (10), as functions of the excitation energy for the  $4d_{3/2,5/2}$  (long dash),  $4f_{5/2,7/2}$  (solid),  $5s$  (dotted),  $5p_{1/2,3/2}$  (chain), and  $5g_{7/2,9/2}$  (short dash) orbitals.

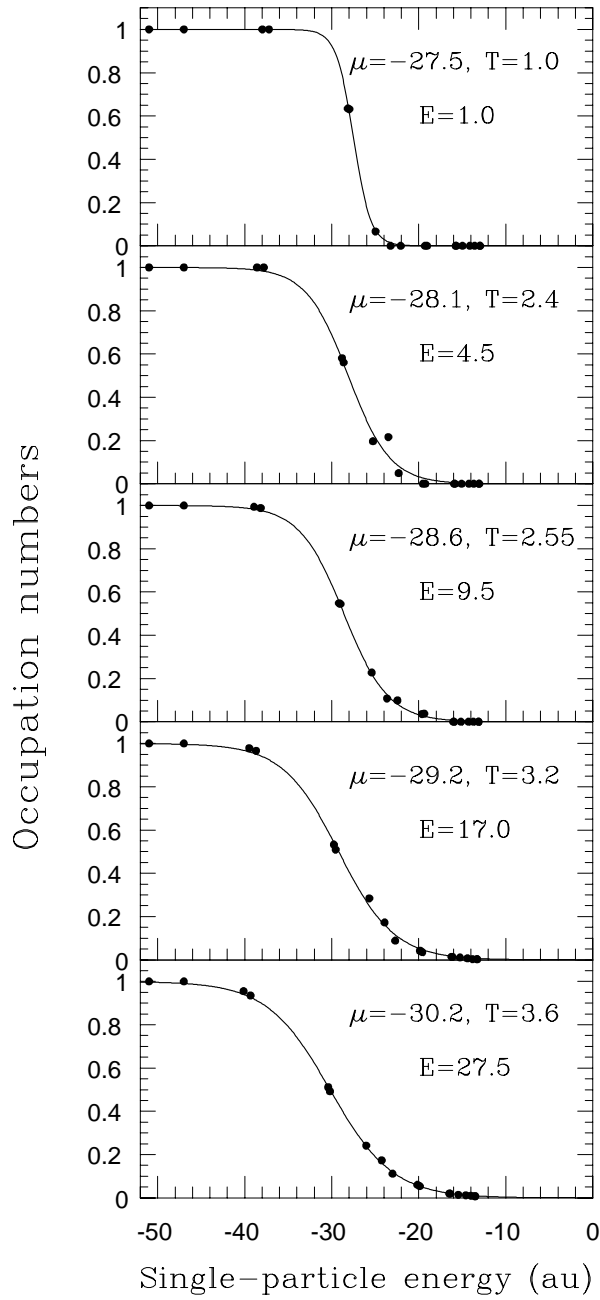


FIG. 7. Orbital occupation numbers in  $\text{Au}^{24+}$  calculated numerically from Eq. (7) at excitation energies  $E = 1, 4.5, 9.5, 17$  and  $27.5$  a.u. (solid circles), and the Fermi-Dirac distributions (solid line) with temperature  $T$  and chemical potential  $\mu$  chosen to give best fits of the numerical data.

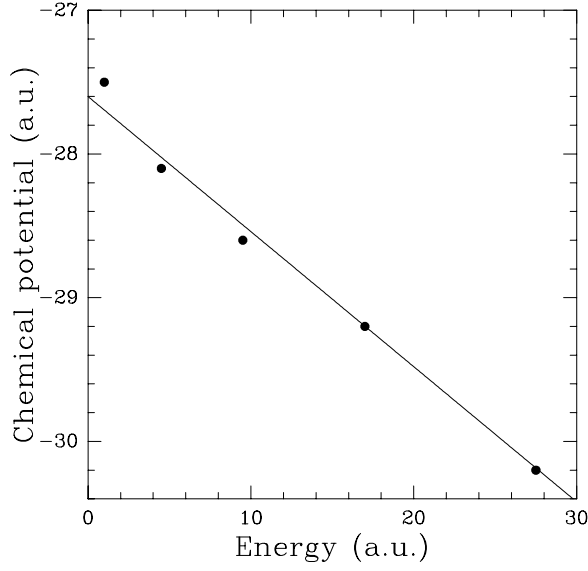


FIG. 8. Chemical potential obtained from the FD distribution fits of the occupation numbers, Fig. 7, as a function of the excitation energy of  $\text{Au}^{24+}$  (solid circles). Solid line is a simple linear fit  $\mu = -27.6 - 0.094E$  a.u.

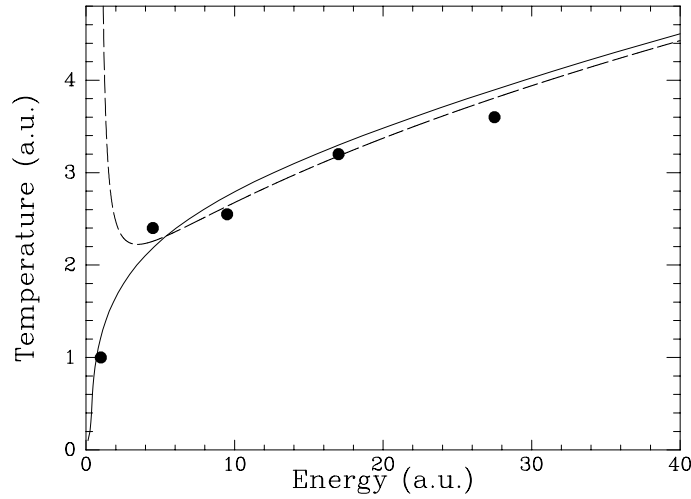


FIG. 9. Temperature vs energy for  $\text{Au}^{24+}$ . Solid line - canonical definition, Eq. (12); dashed line - statistical physics definition, Eq. (13), which uses the density fit (5); solid circles - Fermi-Dirac fits of the occupation numbers.